Stochastic modeling of fluid acceleration on residual scales and dynamics of suspended inertial particles in turbulence

Vladimir Sabelnikov,[1] Alexis Barge,[2] and Mikhael Gorokhovski[2,*]

[1]*ONERA—The French Aerospace Laboratory, F-91761 Palaiseau, France; Central Aerohydrodynamic Institute (TsAGI), 140180 Zhukovsky, Moscow Region, Russian Federation*

[2]*Laboratoire de Mecanique des Fluides et d'Acoustique, CNRS - Ecole Centrale de Lyon-INSA-Universite Claude Bernard Lyon 1, 69134 Ecully, France*

(Received 31 July 2018; published 4 April 2019)

In numerical simulations with highly turbulent flows, the smallest scales are filtered; thereby, the effects of intermittency on those scales are neglected. When the flow is loaded by heavy small particles, the decimation of rapid changes in the velocity may lead to wrong results. This paper provides an approach to take account of subfiltered events of strong velocity jumps on the motion of heavy small particles. The idea is to force the filtered Navier-Stokes equations by a stochastic acceleration term with statistical properties identified by experiments and DNS. To this end, the stochastic model for supplemented acceleration contains the lognormal stochastic process for its norm (with long-range correlations) and the new stochastic model for the acceleration direction (with short-range correlations). The latter represents the Ornstein-Uhlenbeck process in Cartesian coordinates with relaxation to the local direction of the resolved vorticity; thereby, the geometry of highly stretched vortical structures is introduced in the designed model. Both stochastic processes depend on the local Reynolds number. The proposed flow model is applied for simulation of the background turbulence in which heavy particles are released and tracked. The assessment of single and two-time statistics of the particle acceleration and velocity clearly illustrates the advantage of the proposed flow model.

DOI: 10.1103/PhysRevFluids.4.044301

I. INTRODUCTION

Often in nature and industrial applications, the solid particles, or droplets, are transported and dispersed by the carrier fluid. In numerical simulations of such two-phase flows, we need to characterize interactions between particles and flow. In most cases, the carrier fluid is highly turbulent. A particular interest in turbulence is the phenomenon of intermittency. The presence of very strong jumps in the velocity records is a manifestation of this phenomenon. According to the analysis [1–6] of experimental and numerical datasets, these jumps, of the order of rms velocity, are associated with the appearance in the flow of thin and very intense vortical structures, called "worms." Such worms persist in time, and contribute to the non-Gaussian statistics of Lagrangian dynamics at small time lags. For large Stokes numbers, the particle response time is large, and the intense but very short-lived fluid solicitations are not of crucial influence on the particle motion [7]. However, at moderate Stokes numbers (examples include direct injection motors, dust/sand storms, pollutants and particulates in turbulent atmosphere), the particle responds to velocity jumps in the carrier flow, and this may play an important role on the particle dynamics. For example, in spray combustion, the vaporizing droplets, subjected to intense accelerations, may provoke

*Corresponding author: mikhael.gorokhovski@ec-lyon.fr

instants when the flame is extinguished. The problem is that in numerical simulations, the scales on which the mentioned above velocity jumps may occur, are usually filtered. Consequently, the computed fluid acceleration becomes under-resolved. This is seen from the following estimation. The acceleration on filtered scales is of the order of $(\overline{a}_k\overline{a}_k)^{1/2} \approx u_\Delta^2/\Delta$, where the filtered increment of velocity, $u_\Delta^2 \approx (\langle\epsilon\rangle\Delta)^{2/3}$, is defined by filtered viscous dissipation $\langle\epsilon\rangle$ and the filter width Δ in the inertial interval $L \gg \Delta \gg \eta$. The acceleration on residual scales can be expressed in turn as $(a_i'a_i')^{1/2} \approx v_\eta^2/\eta$, where the Kolmogorov velocity is $v_\eta^2 \approx (\langle\epsilon\rangle\eta)^{2/3}$. Then it is seen that for the high Reynolds number $\mathrm{Re}_t = \sigma_u L/\nu$, the discarded acceleration on residual scales may be significantly greater than the filtered one: $(a_i'a_i')/(\overline{a}_k\overline{a}_k) \approx (\Delta/\eta)^{2/3}$. Here L is the integral scale, σ_u denotes the root-mean-square velocity, ν is the viscosity, and η is the Kolmogorov scale. From the other side, alternatively to LES approaches, there are also statistical mean-field models of flow, developed along with RANS approaches, such as the method of transported probability density function (PDF) [8]. The latter was further extended for simulation of polydispersed two-phase flows (useful reviews are provided in Refs. [9,10]). Nonetheless, accounting in this approach for intermittency effects, and in the framework of interaction with an inertial particle, is a difficult task.

Our objective in this paper is to assess a simple flow model in which the occurrence of intense acceleration events on residual scales is accounted for in the dynamics of heavy, but small particles (of few μm size), released and tracked in the background turbulence. The approach represents the further development of our previous work [11,12], in which the filtered Navier-Stokes equations were supplemented by the stochastic acceleration on residual scales. The stochastic model for this acceleration was deemed to represent the statistical properties from experimental observations [13–15]. This approach was referred to as LES-stochastic subgrid acceleration model (SSAM). Namely, along with the lognormal stochastic process for the norm of the residual acceleration, the direction of the latter was simulated as a random walk: The new acceleration direction was sampled randomly after each passage of the Kolmogorov time τ_η. In Ref. [16], LES-SSAM was extended for the channel flows, with and without heavy particles. Here again the random walk model was employed for direction of the residual acceleration: the direction was defined by random positions, spreading progressively on the unit sphere by the Wiener process, with τ_η^{-1} as the diffusion coefficient. The incompleteness of random walk models for the acceleration direction is as follows. As time advances, the change of the acceleration vector has a typical correlation timescale determined by the autocorrelation function. The DNS and experiments show that this typical timescale is of the order of the Kolmogorov time. However, in the random walk models, the autocorrelation timescale is not a physical parameter, it goes to zero with reducing the time interval. This motivates to construct the Ornstein-Uhlenbeck process for the acceleration direction. Recently, the Ornstein-Uhlenbeck process was designed in Ref. [17] for the direction of a heavy particle acceleration. Following generalization of the Ornstein-Uhlenbeck process to the spherical case [18,19], the angular velocity on the unit sphere was simulated in Ref. [17] by the Langevin equation, evolving the displacement of the unit vector by its cross product with the angular velocity vector; the latter was stochastically simulated on each time step. We found that for the unit vector components, this model may often lead to negative or increasing with time autocorrelation functions. Therefore, our approach here is different. We derived and integrated the stochastic equation directly for the unit vector components in Cartesian coordinates. Physically, our motivation was to highlight the geometry of vortical flow patterns, apparently responsible for universality in small-scale turbulence [20]. To this end, the stochastic equation for the unit vector components was completed by the relaxation term towards the direction of the vorticity vector, locally computed in the flow on filtered scales. This model and the method of the stochastic integration are introduced in Sec. II, and the details are presented in the Appendix. In Sec. III, we assess the efficiency of the proposed flow model in prediction of the dynamics of inertial particles suspended in the box turbulence. Namely, we compared the statistics of the particle acceleration and velocity in the carrier flow obtained by DNS on $N^3 = 512^3$ grid nodes with those statistics when the flow was simulated on a coarse grid ($N^3 = 32^3$) by revised LES-SSAM, by LES-SSAM with the random walk model [16] for the

residual acceleration direction, and by standard LES, alternatively. The particles with the moderate Stokes number were considered. Section IV represents concluding remarks.

II. REVISED LES-SSAM APPROACH

The LES-SSAM approach is based on the stochastic Navier-Stokes equation, in which along with the eddy-viscosity term, the stochastic term is included to represent the stochastic acceleration on residual scales:

$$\frac{\partial \hat{u}_i}{\partial t} + \hat{u}_k \frac{\partial \hat{u}_i}{\partial x_k} = -\frac{1}{\rho}\frac{\partial \hat{P}}{\partial x_i} + \frac{\partial}{\partial x_k}\left[(\nu + \nu_t)\left(\frac{\partial \hat{u}_i}{\partial x_k} + \frac{\partial \hat{u}_k}{\partial x_i}\right)\right] + a_i^*, \tag{1}$$

$$\frac{\partial \hat{u}_k}{\partial x_k} = 0. \tag{2}$$

Here, the pressure $\hat{P}$ maintains the solenoidality of the instantaneous velocity field $\hat{u}_i$, and ν_t is the Smagorinsky eddy-viscosity. From experimental studies [13–15] and DNS [21–23], it is known that the norm and the direction of the Lagrangian acceleration are separated by significantly different autocorrelation times. The correlation of the acceleration norm is characterized by integral times, while the acceleration itself is correlated on short times. With increasing the Reynolds number, the acceleration distribution exhibits heavier tails. The idea in LES-SSAM [12] is to prescribe the aforementioned statistical properties directly to the forcing term a_i^*. In this way, the stochastic source term a_i^* was introduced in Ref. [12] as a product of two independent stochastic variables, the norm of acceleration $a^*(t)$ and its components of direction $e_i(t)$:

$$a_i^* = a^*(t)e_i(t), \quad e_i e_i = 1, \tag{3}$$

i.e., the joint probability density function was represented by the product of marginal probability density functions: $P(a, e_i) = P(a)P(e_i)$. In the framework of the Kolmogorov-Oboukhov 62 theory [24], and applying the Ito transformation to the Pope-Chen stochastic equation for viscous dissipation ϵ [25], the following lognormal process, correlated on integral times T, was proposed in Ref. [12] for the acceleration norm:

$$da^* = -a^*\left(\ln\frac{a^*}{a_\eta} - \frac{3}{16}\sigma^2\right)\frac{dt}{T} + \frac{3}{4}a^*\sqrt{\frac{2\sigma^2}{T}}dW(t). \tag{4}$$

Here, $dW(t)$ is the increment of standard Brownian process, i.e., $\langle dW\rangle = 0$, $\langle (dW)^2\rangle = dt$, the dispersion σ^2 depends on the local Reynolds number $\mathrm{Re}_\Delta = \nu_t/\nu$ as $\sigma^2 = \mu \ln \mathrm{Re}_\Delta^{3/4}$, and $a_\eta = \langle\epsilon\rangle^{3/4}/\nu^{1/4}$ is the Kolmogorov acceleration. Additionally, $d\overline{a^*} = 0$ and $d\overline{(a^*)^2} = 0$. In this paper, we replace the random walk model for $e_i(t)$, used in previous LES-SSAM [11,12] and [16] by the new stochastic model. This model is consistent with two physical assumptions.

First, in the framework of the Ornstein-Uhlenbeck process, the new model retains the typical autocorrelation timescale. In Sec. III, this timescale is supposed to be equal to the Kolmogorov time τ_η, in accord with Refs. [13–15]. In Cartesian coordinates, the following form of the Langevin equation for each component can be written in terms of Ito calculus:

$$de_i = -2T_{\mathrm{Diff}}^{-1}e_i dt + (\delta_{ij} - e_i e_j)\sqrt{2T_{\mathrm{Diff}}^{-1}}dW_j, \quad \langle dW_i dW_j\rangle = \delta_{ij}dt, \tag{5}$$

where δ_{ij} is the Kronecker δ, $W_j (j = 1, 2, 3)$ represents independent components of the Brownian vector process, and T_{Diff} is the autocorrelation timescale. Since, to our knowledge, the stochastic equation for the unit direction vector in Cartesian coordinates and the corresponding simulation of the Ornstein-Ulhenbeck process are not well explored in the literature, we derived different equivalent forms of this equation (given in the Appendix) and suggest the method of its integration. It is seen that Eq. (5) is a nonlinear stochastic ordinary differential equation with multiplicative noise. It can be shown that this equation preserves the norm $e_i(t)e_i(t) = 1$ at any instant, if initially

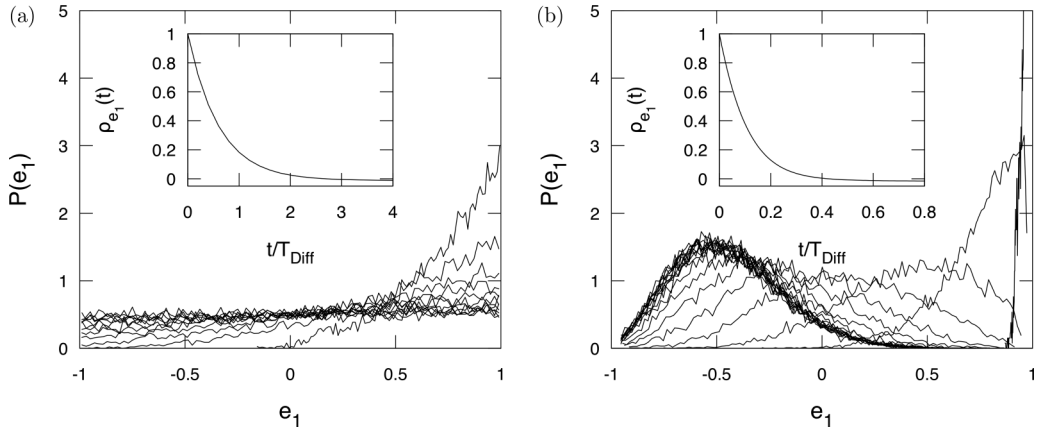

FIG. 1. (a) Results from integration of Eq. (6): PDF evolution in time of the unit vector component (shown at each 10 time steps) and the autocorrelation function; $T_{\rm Diff} = 0.01$; number of released stochastic particles is 10 000; number of time steps 500; the final time is equal to one. (b) Results from integration of Eq. (8): the PDF evolution in time (shown at each 10 time steps) and the autocorrelation function for the unit vector component e_1; $h_1 = -0.5$; $T_{\rm Diff} = 0.1$; $T_{\rm rel} = 0.01$; number of released stochastic particles is 10 000; number of time steps 500; the final time is equal to one.

that norm is equal to unity, $e_i(0)e_i(0) = 1$ (see the Appendix). Since the Stratonovich calculus enjoins the classical rules of differential analysis, it is easier to integrate Eq. (5) into the framework of Stratonovich calculus. In Stratonovich sense, the differential de_i in Eq. (5) admits the following equivalent form:

$$de_i = \sqrt{2T_{\rm Diff}^{-1}}\epsilon_{ijk}dW_j \circ e_k, \tag{6}$$

where ϵ_{ijk} is the Levi-Civita symbol, and the symbol $\circ$ denotes Stratonovich calculus. Here also, multiplying both sides by e_i, the right-hand side becomes zero, and hence, $d(e_ie_i) = 0$. For integration of Eq. (5), the midpoint method (see the Appendix) appears to be simple, fast, and effective. An illustration of this integration—the evolution of PDF of the unit vector component e_i and its autocorrelation function—is show in Fig. 1(a). It is seen that the PDF relaxes progressively towards the uniform distribution. The second assumption for the stochastic model of direction concerns its relaxation towards the direction of the locally resolved vorticity vector; thereby, we try to take into account the geometry of aforementioned vortical flow structures, emphasized in Refs. [1,2,4], and especially in Ref. [20]. Our DNS confirms this assumption in the following way. The DNS of turbulence with simulation of fluid particle motion is performed in the periodic cubic box of size $L = 2\pi$ m, discretized by 512^3 grid points. The numerical approach [26,27] includes the pseudospectral methods in space; the nonlinear terms are directly solved with the classical 2/3 rule to avoid aliasing errors, and the linear terms are implicitly calculated. The integration in time is performed by the second order Runge-Kutta scheme. The code was developed and tested in Ref. [28]. Once the statically stationary state of the turbulence is attained, we subdivide the computational box into identical cubic cells, of a size greater than the mesh size. For each cubic cell we form the block direction of the acceleration of fluid particles, located in the considered cell, and the block direction of the vorticity seen by those particles. Then we compute the correlation coefficient between these two directions, and we repeat the same procedure for cubic cells of greater size. For $\mathrm{Re}_\lambda = 140$ in Fig. 2, the correlation coefficient is presented for different sizes $5 \leqslant l/\eta \leqslant 120$ of cubic cells. The mesh used in LES hereafter corresponds to $\Delta/\eta = 23$. It is seen that starting from the cell size of the order of resolved LES scales, both block directions become significantly correlated. This implies that the direction of the acceleration averaged over the cubic

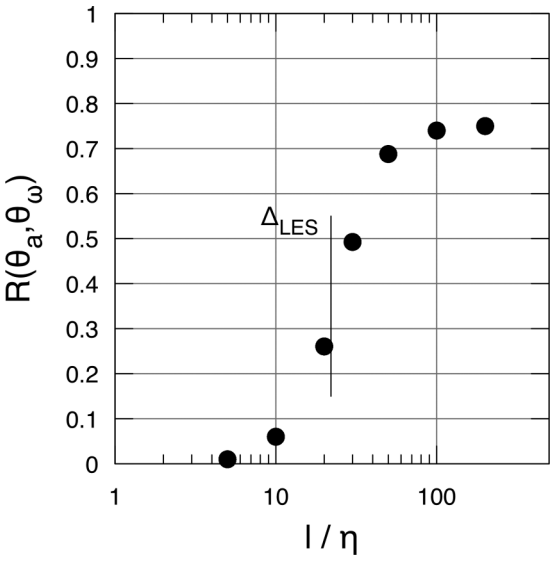

FIG. 2. DNS of box turbulence, $\mathrm{Re}_\lambda = 140$; the correlation coefficient between block directions of acceleration of fluid particles and vorticities seen by those particles in the block; l/η indicates different sizes of blocks. θ_a is the direction angle of the particle acceleration vector and θ_ω is the direction angle of the vorticity vector seen by the particle.

cell of size of the filter width Δ tends to be aligned with the block direction of the vorticity seen by the fluid particles. In this context, we modify Eq. (5) by adding a relaxation term toward the presumed direction:

$$de_i = -h_{\perp,i}T_{\mathrm{rel}}^{-1}dt - 2T_{\mathrm{Diff}}^{-1}e_i dt + (\delta_{ij} - e_i e_j)\sqrt{2T_{\mathrm{Diff}}^{-1}}dW_j \;\; ; \;\; \langle dW_i dW_j\rangle = \delta_{ij}dt \tag{7}$$

where h_i are the components of the presumed direction, thought of in Section III as components of the resolved vorticity direction; T_{rel} is the typical time of relaxation, and $h_{\perp,i} = h_i - (h_j e_j)e_i$ denotes the projection form. In terms of Stratonovich calculus, Eq.(7) has the following form:

$$de_i = -h_{\perp,i}T_{\mathrm{rel}}^{-1}dt + \sqrt{2T_{\mathrm{Diff}}^{-1}}\epsilon_{ijk}dW_j \circ e_k. \tag{8}$$

The norm $e_i(t)e_i(t) = 1$ in Eqs. (7) and (8) is also preserved. Using again the midpoint method, the first term in Eq. (8) can be updated by implicit approximation (see the Appendix). An example of the PDF evolution in time issued from integration of Eq. (8), where $h_1 = -0.5$ is used, and the autocorrelation functions are given on Fig. 1(b). As expected, the PDFs evolve in time to the long-time stationary Gaussian-shape distribution. Equations (1)–(4) and (8) constitute the flow model referred to as revised LES-SSAM.

According to measurements in Refs. [13–15], the Lagrangian velocity increment is normally distributed at large time lags, while at small time lags it exhibits the non-Gaussian distribution with stretched tails. This is the way in which the intermittency in Lagrangian variables is manifested: The large time lags are associated with the particle velocity, usually conformed to the central limit theorem, whereas statistics at small time lags represent the acceleration of the particle, a highly intermittent parameter when the Reynolds number is large. The ability to reproduce these properties by LES-SSAM for fluid particles is illustrated in Fig. 3. In this figure, we compared numerical results from DNS, standard LES, LES-SSAM [16] with random walk model for direction of the residual acceleration (referred hereafter to as LES-SSAMRW), and LES-SSAM revised. In the latter, T_{rel}^{-1} in Eq. (8) is thought of as the characteristic rate of strain, resolved on filtered scales,

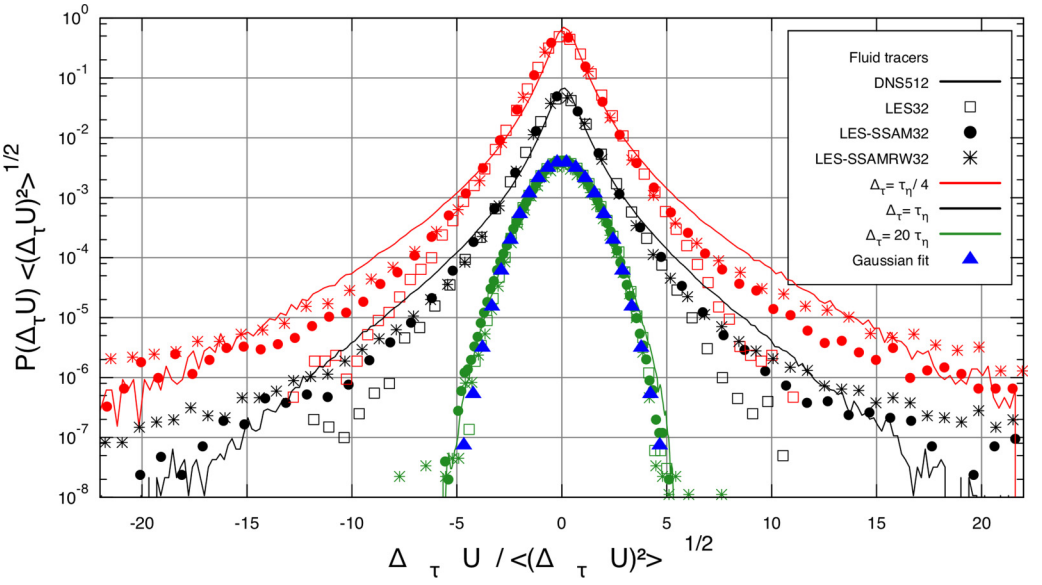

FIG. 3. Fluid tracer velocity increments at different time lags in the box turbulence: DNS (—), standard LES (□); LES-SSAMRW [16] (∗); LES-SSAM revised with Eq. (8) (•); (▲) Gaussian fit. PDFs are shifted toward the lower part with increasing of time lag.

$S \equiv (2\hat{S}_{ik}\hat{S}_{ik})^{1/2}$, $\hat{S}_{ik} = (\frac{\partial \hat{u}_k}{\partial x_i} + \frac{\partial \hat{u}_i}{\partial x_k})/2$, and h_i in Eq. (8) represents the components of the direction of the resolved vorticity vector. The PDFs are shifted toward the lower part with increasing of time lag. The Reynolds number in the background turbulence is $\mathrm{Re}_\lambda = 140$. It is seen that at large time lags (of the order of 20 Kolmogorov's times, given here by DNS, as $\tau_\eta = \sqrt{\nu/\langle\epsilon\rangle} = 0.06$ s), all four approaches display the velocity increment being normally distributed. At smaller time lags, the velocity increment PDF in DNS develops a growing central peak with progressively

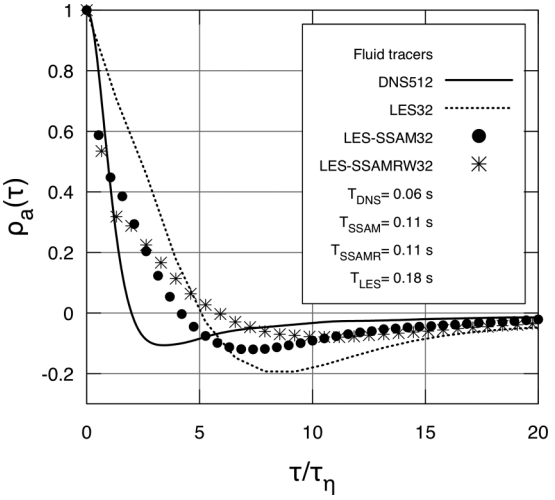

FIG. 4. The autocorrelation function of the fluid particle acceleration in the box turbulence given by DNS (—), LES-SSAMRW [16] (∗), LES-SSAM revised (•); $\mathrm{Re}_\lambda = 140$. For comparison, the autocorrelation function of the Lagrangian time derivative of the filtered velocity from LES (- - -) is also presented.

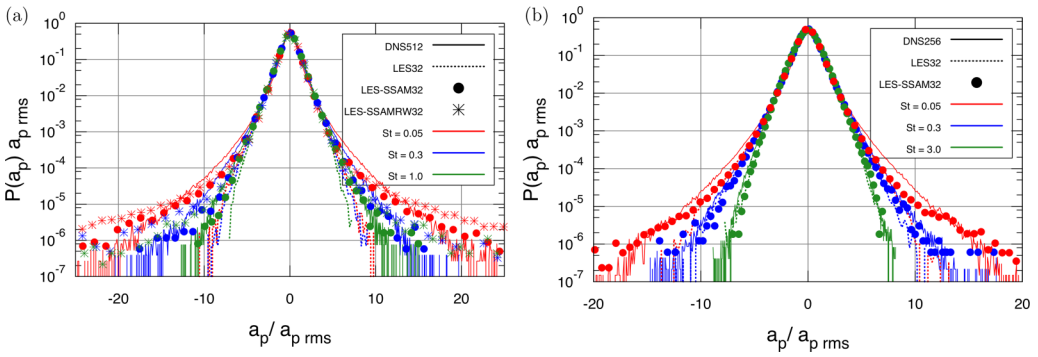

FIG. 5. Standardized PDF's of the particle acceleration, St = 0.05, 0.3, 1.0, from DNS (—), standard LES (- - -), LES-SSAMRW (∗), and LES-SSAM revised (•). (a) $\mathrm{Re}_\lambda = 140$. (b) $\mathrm{Re}_\lambda = 70$.

stretched tails: The small amplitude events alternate with events when the particle is subjected to intense accelerations. In contrast to the case of standard LES, distributions from LES-SSAM revised and LES-SSAMRW [16] reproduce those tails. However, using LES-SSAMRW, those tails become lightly stretched in comparison with distributions from DNS and LES-SSAM revised. This may result in overestimation of large fluctuations of the inertial particle acceleration. In Fig. 4, we compare the autocorrelation function of the fluid particle acceleration, $\rho_{a_p}(\tau) = \langle a_{p,k}(t+\tau)a_{p,k}(t)\rangle / \langle a_{p,k}(t)a_{p,k}(t)\rangle$, in the flow from DNS with the autocorrelation function of the Lagrangian time derivative of the velocity from LES-SSAMRW, LES-SSAM revised, and standard LES. It should be noted that this derivative is not the acceleration of fluid particle, and this comparison takes the formal character. Nevertheless, it is seen that at small time lags (of the order of Kolmogorov's time), the computed autocorrelations from both LES-SSAM follow closely the autocorrelation function of the fluid particle acceleration from DNS. For larger time lags, the autocorrelations from LES-SSAM move slightly away from DNS, being nevertheless closer to DNS than the autocorrelation function from standard LES. The stronger resemblance with DNS of the autocorrelation function from LES-SSAM revised is also seen in comparison with the case of LES-SSAMRW. The impact of small-scale extreme events (stretched tails in Fig. 3) on the inertial particle motion is demonstrated in the next section.

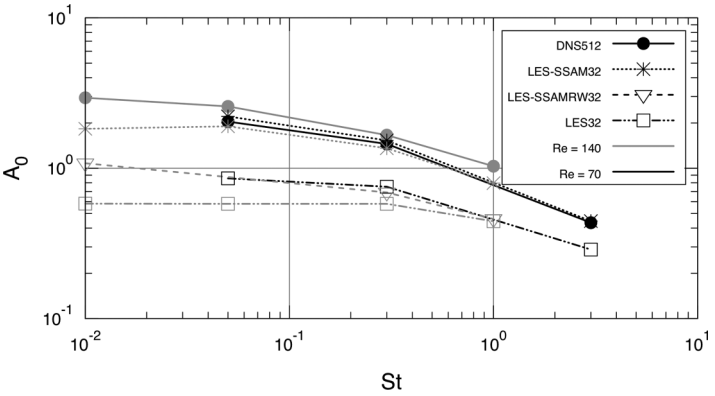

FIG. 6. Acceleration variance as a function of the Stokes number in the dimensionless form $A_0 = \langle a_p^2\rangle \langle \epsilon^{-3/2}\rangle \nu^{1/2}$; $\mathrm{Re}_\lambda = 70,\ 140$. Results from DNS, standard LES, LES-SSAMRW, and LES-SSAM revised.

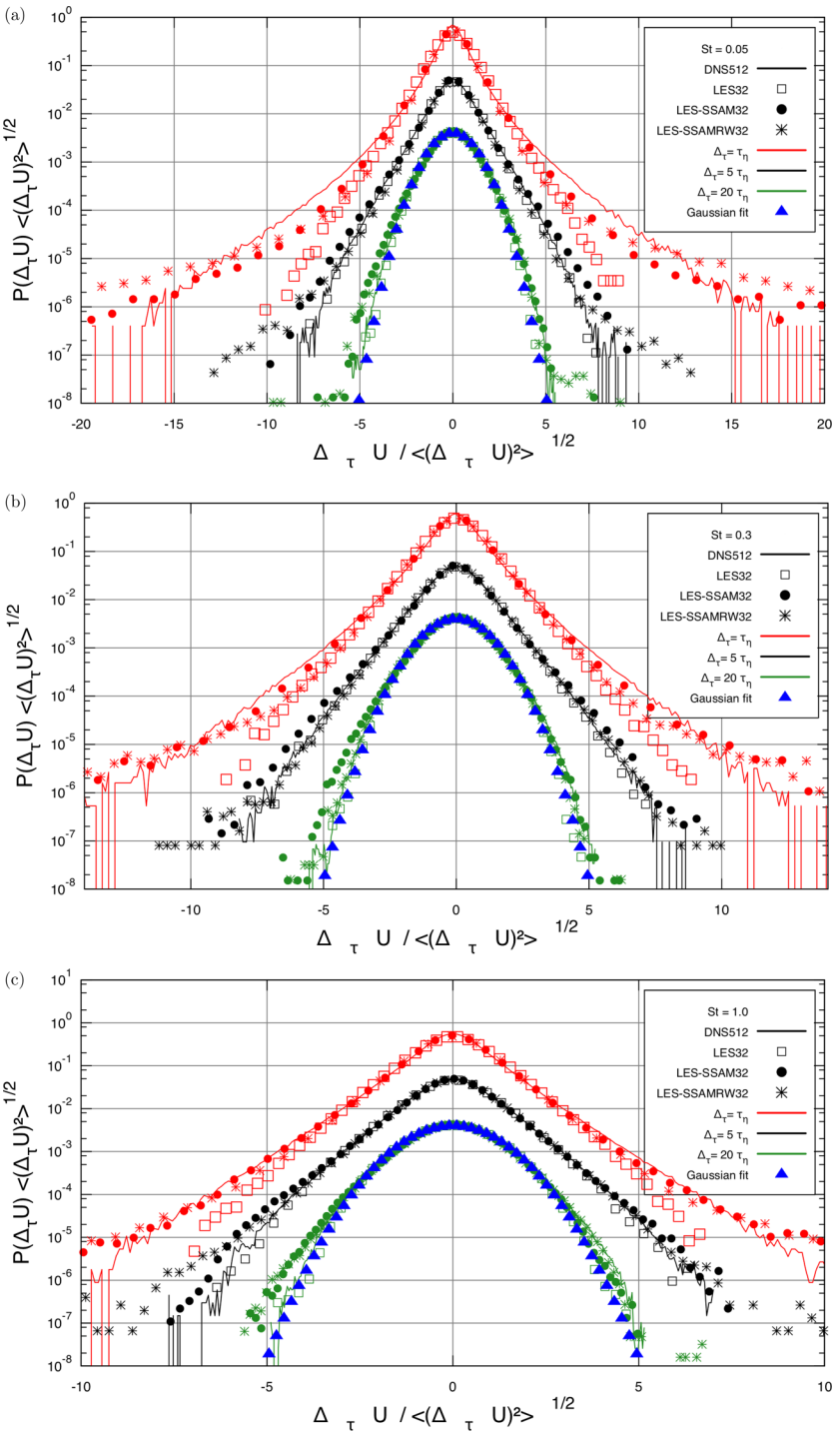

FIG. 7. (a–c) Distributions of the heavy particle velocity increment at different time lags and different Stokes numbers: St $= 0.05,\ 0.3,\ 1.0$, from DNS (—), standard LES (□), LES-SSAMRW (∗), and revised LES-SSAM (•). The background turbulence: $\mathrm{Re}_\lambda = 140$; PDFs are shifted toward the lower part with increasing the time lag.

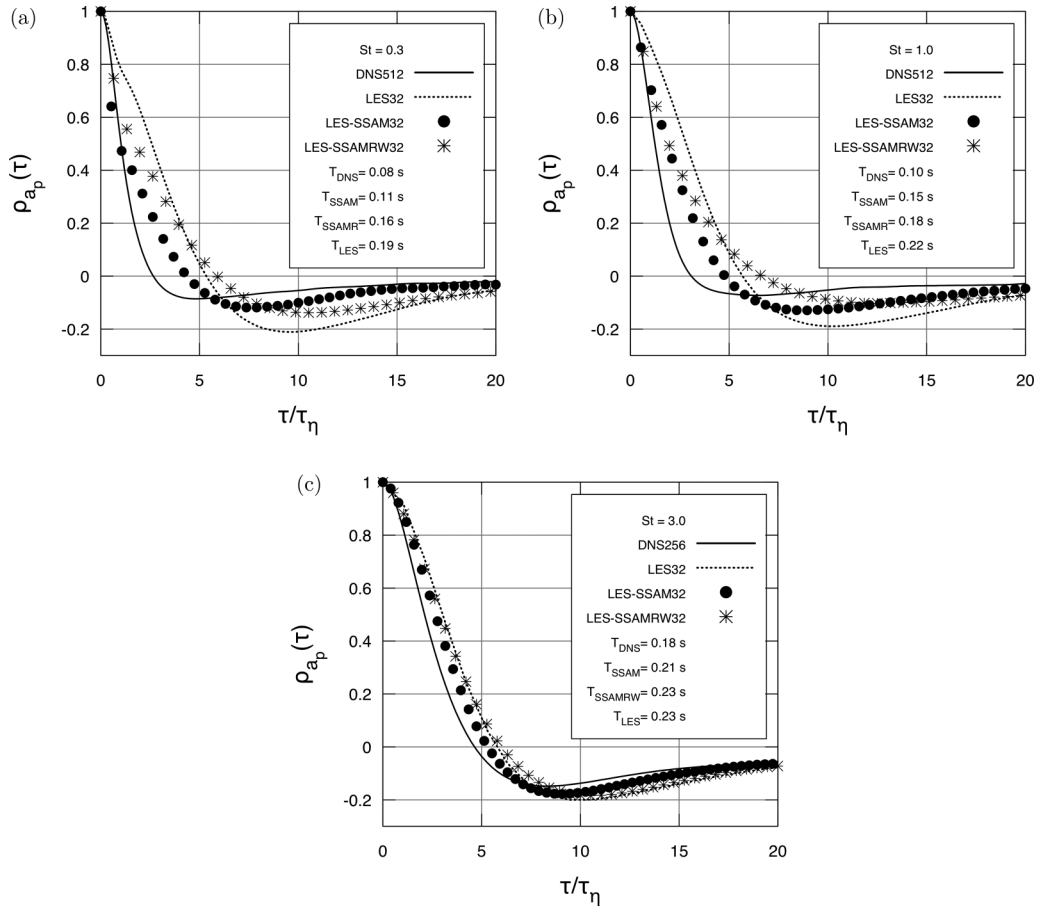

FIG. 8. (a, b) The autocorrelation function of the heavy particle acceleration at the moderate Stokes number, St = 0.3, 1.0, in the box turbulence given by DNS (—), standard LES (- - -), LES-SSAMRW (∗), and LES-SSAM revised (•); $\mathrm{Re}_\lambda = 140$. (c) St = 3.0; $\mathrm{Re}_\lambda = 70$.

III. STATISTICS OF HEAVY PARTICLES: ASSESSMENT OF REVISED LES-SSAM

For the test case, we performed DNS of the box turbulence with inertial particles (parameters of DNS are mentioned in the previous section). The particles were injected when the flow reached its statistically stationary state. The motion of inertial particle is governed by the Stokes drag force:

$$\frac{d\mathbf{u}_p}{dt} = \frac{\mathbf{u} - \mathbf{u}_p}{\tau_p}, \quad \tau_p = \frac{\rho_p d_p^2}{18\rho\nu} s, \tag{9}$$

where $\mathbf{u}_p$, ρ_p, d_p are the particle velocity, density, and diameter, respectively, and $\mathbf{u}$ refers to the velocity of the carrier phase interpolated at the particle position. We compared DNS data with those numerical simulations when the fluid velocity at the particle position in Eq. (9) is given by standard LES, by LES-SSAMRW, or by the revised LES-SSAM, alternatively. The moderate Stokes number is taken: $\mathrm{St} = \tau_p/\tau_\eta = 0.05,\ 0.3,\ 1,\ 3.0$. Hereafter, T_L and τ_η are the correlation time of the fluid tracer velocity and the Kolmogorov time, respectively, both computed by DNS. Figure 5 shows the normalized distribution of inertial particles acceleration in the background turbulence at two Reynolds numbers, $\mathrm{Re}_\lambda = 70$ and $\mathrm{Re}_\lambda = 140$. For both Reynolds numbers, the DNS data display the broad tails in distributions. These tails are more stretched as the Reynolds number

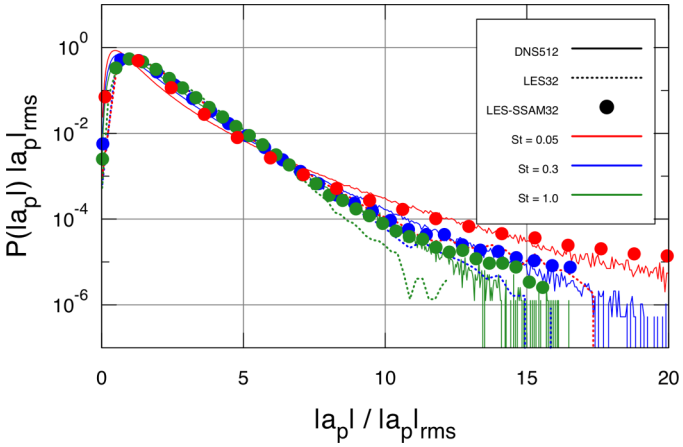

FIG. 9. Standardized PDFs of the acceleration norm of the particle at St = 0.05, 0.3, 1.0 from DNS (—), standard LES (- - -), and LES-SSAM revised (•). $\mathrm{Re}_\lambda = 140$.

is increased. Also, for the decreased Stokes number, the tails are broader, indicating the events of intense acceleration of the particle in response to strong velocity jumps in the carrier fluid. This is correctly represented by LES-SSAM revised, whereas distributions, when standard LES is used, are characterized by significantly reduced tails. It is also seen that using standard LES, the effect of the turbulent Reynolds number on the particle acceleration is not remarkable. These distributions are also compared with those from LES-SSAMRW. It is seen that at small Stokes number, the LES-SSAM with random walk leads to excessively stretched tails in the normalized distribution of acceleration. We also compared the variance of the inertial particle acceleration obtained in considered approaches. This is shown in Fig. 6, where for $\mathrm{Re}_\lambda = 70$ and $\mathrm{Re}_\lambda = 140$, the acceleration variance, as a function of the Stokes number, is given in the dimensionless form $A_0 = \langle a_p^2 \rangle \langle \epsilon^{-3/2} \rangle \nu^{1/2}$. It is seen that the particle acceleration variance is better predicted when the flow is simulated by LES-SSAM revised, in comparison to standard LES, and LES-SSAMRW. Another demonstration of the efficiency of revised LES-SSAM to take into account the velocity jumps on the particle motion is given in Fig. 7. Here, using the flow data from DNS, standard LES, LES-SSAMRW, and revised LES-SSAM, the PDF of the increment of the heavy particle velocity is compared at different time lags, for $\mathrm{Re}_\lambda = 140$ and for three values of the Stokes number $\mathrm{St} = 0.05,\ 0.3,\ 1.0$. At these moderate Stokes numbers, it is seen from DNS that the particle responds vigorously to strongest and short-lived fluctuations of the velocity in the carrier fluid. The strong non-Gaussianity on time lags, of the order of few Kolmogorov's times, is a manifestation of such behavior of the particle, to some extent similar to fluid tracer in Fig. 3. As expected, the tails in the velocity increment PDF are less extended for larger Stokes numbers. These effects are predicted correctly when revised LES-SSAM is used, whereas in the case of standard LES, the distribution of the particle velocity increment at time lags of one and five Kolmogorov's times remains almost invariant. It is seen also in this figure that at smallest time lags and smallest Stokes numbers, the contribution of large fluctuations in LES-SSAMRW may be more significant than in DNS and LES-SSAM revised. When the interval is large enough (20 Kolmogorov's times here), the velocity increment distribution is Gaussian in all considered approaches, including the case of the standard LES. The comparison of the autocorrelation function of the heavy particle acceleration $\rho_{a_p}(\tau) = \langle a_{p,k}(t) a_{p,k}(t+\tau) \rangle / \langle a_{p,k}(t) a_{p,k}(t) \rangle$, with $\rho_a(0) = 1$ in the carrier turbulent field from DNS, standard LES, LES-SSAMRW, and LES-SSAM revised is presented in Fig. 8 for $\mathrm{St} = 0.3,\ 1,\ 3.0$. Similar to Fig. 4, it is seen that at small time lags, the autocorrelation function from both LES-SSAM approaches are close to DNS data. For larger time lags, there is a slight difference with DNS, but the particle acceleration autocorrelation function and the

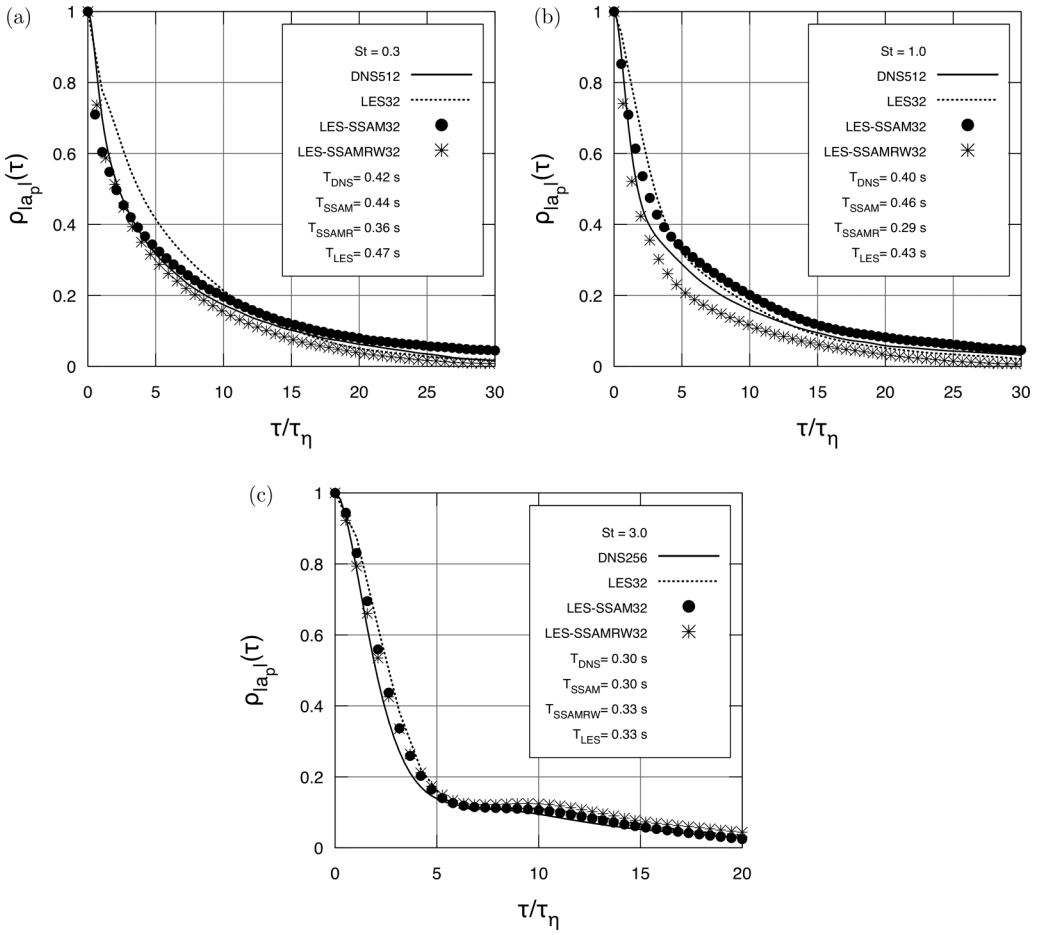

FIG. 10. (a, b) The autocorrelation function of the acceleration norm of the heavy particle at the moderate Stokes number, St = 0.3, 1.0, from DNS (—), standard LES (- - -), LES-SSAMRW (∗), and LES-SSAM revised (•); $\mathrm{Re}_\lambda = 140$. (c) St = 3.0; $\mathrm{Re}_\lambda = 70$.

autocorrelation time are predicted by revised LES-SSAM better than in the case of LES-SSAMRW. Although the autocorrelation time is mainly determined here by the Kolmogorov time, it is seen that with increasing the Stokes number, the particle acceleration is longer correlated: The direction of the heavier particle, being changed by helical structures, persists for a longer time. On the other side, the particle with a larger response time is less sensitive to extreme fluctuations of its acceleration amplitude. This is seen in Fig. 9 for the acceleration norm distributions of the particle at different Stokes numbers. Here also, contrary to standard LES, the case with LES-SSAM revised follows mostly the prediction from DNS of strong accelerations events. In Fig. 10, the autocorrelation function of the particle acceleration norm $\rho_{|a_p|}(\tau) = \langle |a_p(t)||a_p(t+\tau)|\rangle / \langle |a_p(t)|^2\rangle$; $|a| = \sqrt{a_{p,1}^2 + a_{p,2}^2 + a_{p,3}^2}$; $\rho_{|a_p|}(0) = 1$, is compared when the turbulent flow is simulated by DNS, standard LES, LES-SSAMRW, and LES-SSAM revised. Similar to the observations for fluid particles, the autocorrelation time of the inertial particle acceleration magnitude is much longer than the autocorrelation time of the acceleration itself. However, the particle response to the short-lived strong fluid solicitations has lesser magnitude for a heavier particle, and thereby the magnitude is probably less correlated for that particle. The DNS data, standard LES, and LES-SSAMRW show the autocorrelation time of the acceleration norm being decreased, as the Stokes number is increased

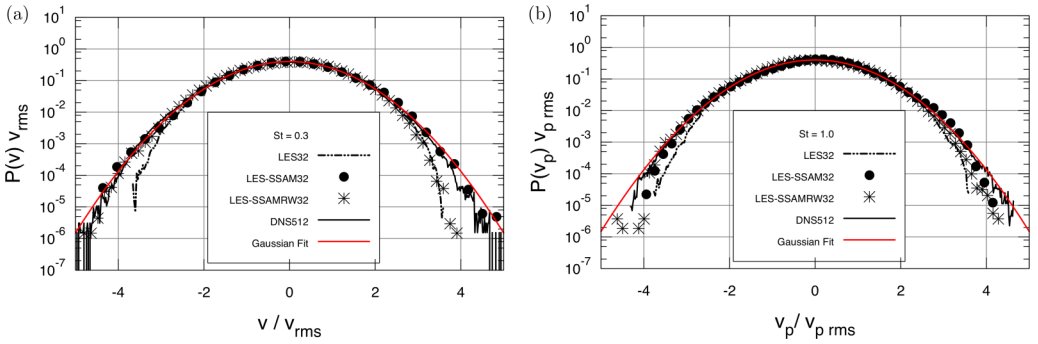

FIG. 11. The particle velocity probability distribution function at St = 0.3, 1.0; $\mathrm{Re}_\lambda = 140$. Comparison from DNS (—), standard LES (- - -), LES-SSAMRW (∗), and LES-SSAM revised (•).

from St = 0.3 to St = 1.0, but not in the case of revised LES-SSAM. Indeed, for St = 0.3, we have $T_{\mathrm{DNS}} = 0.42$ s; $T_{\mathrm{SSAM}} = 0.44$ s; $T_{\mathrm{SSAMRW}} = 0.36$ s; $T_{\mathrm{LES}} = 0.47$ s; and for St = 1.0, we have $T_{\mathrm{DNS}} = 0.4$ s; $T_{\mathrm{SSAM}} = 0.46$ s; $T_{\mathrm{SSAMRW}} = 0.29$ s; $T_{\mathrm{LES}} = 0.43$ s. This deficiency of the revised LES-SSAM is probably due to enforced alignment of the particle acceleration with the vorticity vector: such a particle with the increased Stokes number responds to solicitations of more correlated turbulent scales in the carrier flow. However, it is also seen, that the revised LES-SSAM matches relatively well the shape of the autocorrelation function from DNS, and that the main contribution to the mentioned discrepancy between the autocorrelation time from DNS and from LES-SSAM revised comes from large times. It is also seen in Fig. 10 that in the case of the higher Stokes number, St = 3.0, the autocorrelation time in LES-SSAM revised follows again the tendency from DNS data, and thereby with the increased Stokes number, from 1 to 3, the autocorrelation time of the acceleration norm is decreased along with DNS. The single and two-time statistics, presented in Figs. 3–10 for the acceleration of particles at St $\leqslant$ 1.0, clearly show that the extreme variations of the fluid velocity on residual scales can be correctly accounted in the framework of LES-SSAM revised. We may also ask: What about the prediction of single and two-time statistics of the velocity itself of those particles? This information is relevant to characteristics of the particle diffusion in

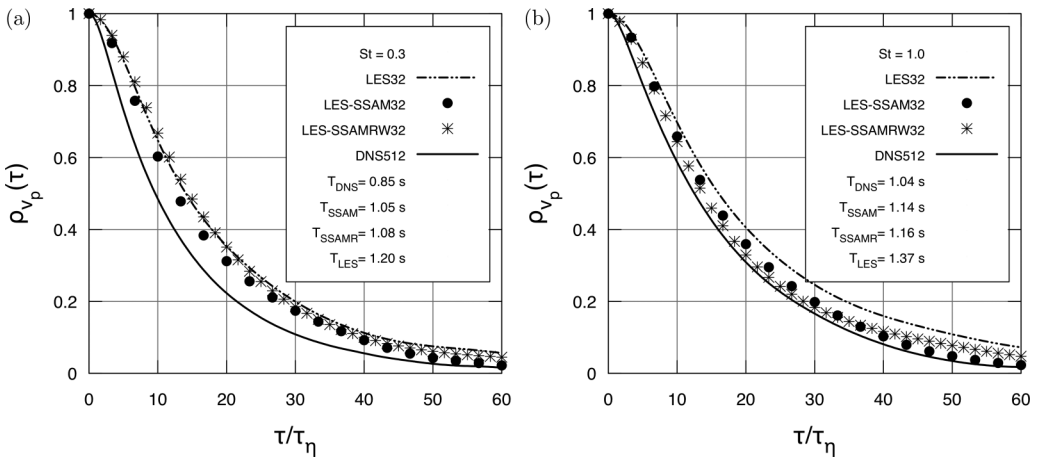

FIG. 12. The Lagrangian velocity autocorrelation function of particle at the moderate Stokes number St = 0.3, 1.0; $\mathrm{Re}_\lambda = 140$. Comparison from DNS (—), standard LES (- - -), LES-SSAMRW (∗), and LES-SSAM revised (•).

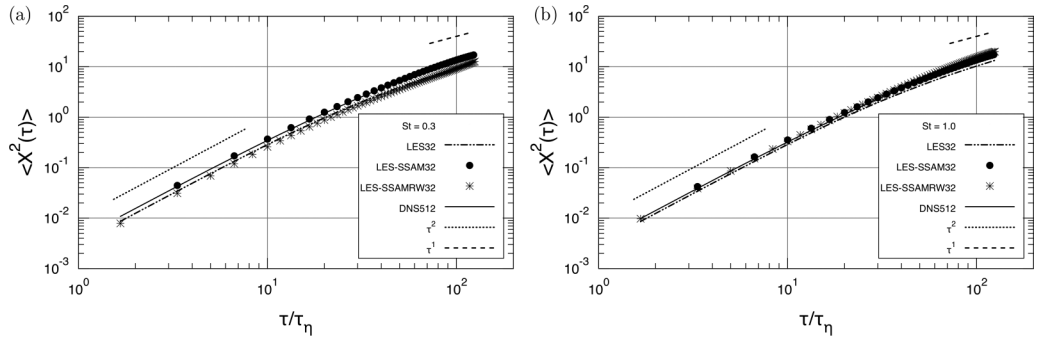

FIG. 13. The mean-square dispersions of particles at St = 0.3, 1.0; $\mathrm{Re}_\lambda = 140$. Comparison from DNS (—), standard LES (– · · –), LES-SSAMRW (∗), and LES-SSAM revised (•). The dashed lines show the ballistic ($\sim\tau^2$) and diffusive ($\sim\tau$) regimes.

stationary turbulence, such as the Lagrangian correlation time, which provides a measure of the Lagrangian velocity memory, and the mean square displacement $\langle X_p^2\rangle$. According to classical works of Taylor [29] and Oboukhov [30], the two main results concerning the fluid particle diffusion in stationary turbulence are: (i) the mean-square displacement is characterized by the ballistic regime for very short times, $t \ll T_L$: $\langle X_p^2\rangle \sim t^2$, and the effective diffusive regime for $t \gg T_L$: $\langle X_p^2\rangle \sim T_L t$; (ii) the particle velocity is a Gaussian process governed by the Fokker-Planck equation. Not much different behavior was demonstrated in DNS of isotropic turbulence ($\mathrm{Re}_\lambda = 47$) in Ref. [31] with heavy particles at St < 1. Applying the considered here approaches for St = 0.3, 1.0, Figs. 11 and 12 show, respectively, the particle velocity probability distribution function and its Lagrangian velocity autocorrelation function. It is seen that LES-SSAM revised matches well the distribution from DNS. The latter represents the Gaussian distribution. This is not the case when standard LES is used. The probability from LES-SSAMRW is slightly distinguishable from the Gaussian distribution. It is also seen that predictions of the Lagrangian correlation time and the velocity autocorrelation function can be improved by LES-SSAM revised. Concerning the mean-square dispersion of particles, it is seen in Fig. 13 that simulations from LES-SSAM revised follow fairly well the results from DNS; log-log presentation indicates ballistic and diffusive regimes,

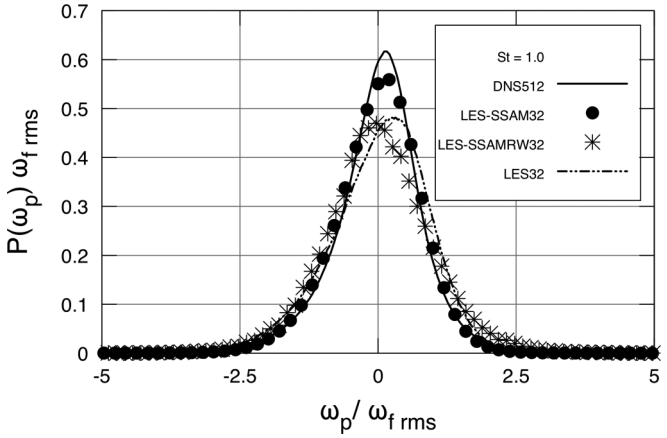

FIG. 14. PDF of the vorticity seen in the flow by the particle at St = 1.0; flow is simulated by DNS (—), standard LES (– · · –), LES-SSAMRW (∗), and LES-SSAM revised (•). ω_p is the vorticity seen by the particle and ω_f is the fluid vorticity.

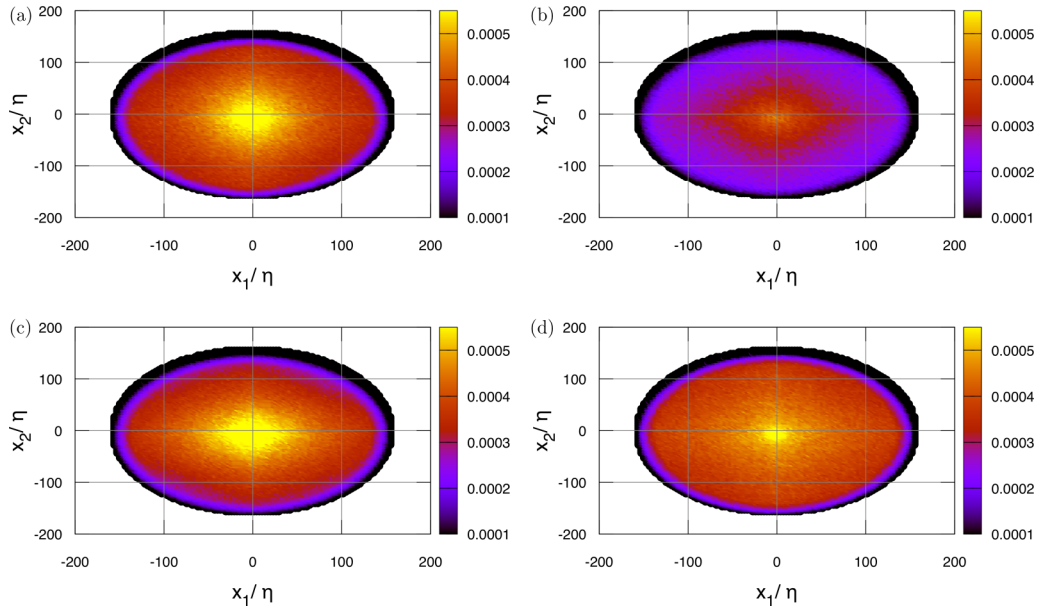

FIG. 15. Spatial distributions of the number fraction of particles located in zones of low vorticity relatively to a considered particle being located in the same vorticity interval; St = 1.0. (a) DNS. (b) Standard LES. (c) LES-SSAM. (d) LES-SSAMRW.

similar to the Taylor law of the fluid particle dispersion. Another question is this: Accounting for turbulent microstructure, may we improve the prediction of large-scale effects on the particle dynamics, such as the trend of inertial particles to stay preferentially in zones of lower vorticity in the carrier flow? To answer this question, the PDF of the vorticity seen by a heavy particle along its trajectory is compared in Fig. 14 at St = 1.0 for flows from DNS, standard LES, LES-SSAMRW, and LES-SSAM revised. It is seen that in comparison to standard LES, the probability of a particle to move preferentially in zones of lower vorticity is well predicted by LES-SSAM. In Fig. 15, this effect is also quantified for ensemble of particles in the given plane. Relatively to the position of a considered particle, which is located in a zone of a low vorticity, we calculated the spatial distribution of the number fraction of all other particles being also located in zones of same vorticity interval. The peak of this proportion, which identifies the tendency of heavy particles to stay in zones of low vorticity, is clearly seen when the flow is given by DNS, and this peak is emerged in LES-SSAM revised similarly to DNS. In contrast, on the same coarse mesh but using standard LES, the distribution of considered proportion is more homogeneous; particles are dispersed in broader regions; the picture in the case of LES-SSAMRW differs also from DNS.

IV. CONCLUSION

In this work, we present a simple flow model in which the presence of occasional very strong velocity jumps is explicitly introduced into background filtered turbulence. The model, referred to here as LES-SSAM revised, is designed specifically for simulation of dispersed two-phase high Reynolds number flows on a coarse grid. To induce the intense short-lived velocity fluctuations on residual scales, the filtered Navier-Stokes equations are supplemented by residual stochastic acceleration, which is governed by stochastic model. The latter is designed in accord with the stochastic properties observed in experiments and DNS. Namely, following our previous LES-SSAM approach, the stochastic model provides for long-range correlation of the acceleration magnitude in the framework of the lognormal process, and gives heavy tails in the PDF of

acceleration, sensitively to the local Reynolds number. The new element in LES-SSAM revised is the model for the acceleration direction, which in the previous versions of LES-SSAM was simulated by a random walk model. The new model is based on the derived stochastic equation for the unit vector components in Cartesian coordinates and represents the Ornstein-Uhlenbeck stochastic process. The new properties of this model are: (i) the autocorrelation time is introduced as a physical parameter, and according to experimental observation, it is associated in the model with the Kolmogorov time; (ii) the relaxation of the acceleration direction to the vorticity vector is introduced in the stochastic equation, and thereby the central role of vortical structures geometry is emphasized in stochastic simulation of small-scale turbulence. Since this model may have numerous applications, the Appendix provides the derivation of equivalent forms of the stochastic equation in terms of Ito and Stratonovich, with the proposal of a numerical scheme of integration.

The single and two-time statistics of the acceleration and the velocity of heavy particles at the moderate Stokes number were assessed in this paper. To this end, particles at $\mathrm{St} = 0.05,\ 0.3,\ 1.0,\ 3.0$ were immersed and tracked in the background turbulence, computed by three approaches: by LES-SSAM revised and standard LES on a coarse grid ($N^3 = 32^3$), and by DNS performed on $N^3 = 512^3$ grid nodes. In comparison to standard LES and to the previous version of LES-SSAM, the results illustrate largely the efficiency of LES-SSAM revised in prediction of non-Gaussianity in the particle behavior, as response to strong velocity jumps in the carrier flow on residual scales. The stretched tails in the PDF of the particle velocity increment, of the particle acceleration and its magnitude, as well as the autocorrelation function of these flow parameters, were predicted accurately. Essential also is that the residual acceleration model from LES-SSAM (for both, the norm and the direction) are shown being controlled by the Reynolds number, while most of the subfilter models in LES are invariant to the local Reynolds number. On the question "predicting better the particle acceleration statistics, could the velocity statistics be improved?" The answer in this paper is also positive. The heavy particle velocity statistics, such as its velocity autocorrelation function, its velocity PDF, and the mean square displacement favored LES-SSAM revised among considered approaches. The ability of LES-SSAM revised to predict better the trend of inertial particles to stay preferentially in zones of lower vorticity in the carrier flow was also demonstrated.

However, the process of particle-turbulence interaction includes so many features that to encompass the sensitivity of LES-SSAM revised to the whole spectrum of those features is a very difficult task. In this work, we just showed that accounting for fine scale dynamics in turbulent flow, one may improve the small-scale properties of the particle motion. To some extent, statistics of the velocity of heavy particles, the trend of these particles to preferential concentration in the low vorticity regions suggest that the large-scale effects may be also improved by LES-SSAM revised. However, the efficiency of LES-SSAM revised is still uncertain in prediction of such complex effects as the coherence in the cluster structures of particles [32], or collisional aggregation due to turbulence [33]; this motivates the further numerical simulations in the future work. It would be also interesting to test LES-SSAM revised in complex conditions: channel flows, vaporizing droplets, rotating particles, particles bigger than the Kolmogorov's scale. The model proposed is simple. The CPU time requirements by this model are not much larger than in the case of standard LES (by a factor 1.33; in the case of LES-SSAM with random walk model, this factor is 1.16). Therefore, the numerical simulations with this model may be also applied to realistic situations, such as simulation of Diesel-like sprays.

ACKNOWLEDGMENTS

A.B. and M.G. gratefully acknowledge the support from The French National Research Agency (ANR) Project No. 13-BS09-0009 LTIF. M.G. gratefully thanks the support from the Center for Turbulence Research, Stanford University, and in particular, the hospitality of Parviz Moin during the Summer Program. V.S. gratefully acknowledges the financial support from ONERA and from

the Grant of the Ministry of Education and Science of the Russian Federation (Contract No. 14.G39.31.0001 of 13.02.2017).

APPENDIX: STOCHASTIC EQUATION FOR THE UNIT VECTOR COMPONENTS—ITO'S AND STRATONOVICH'S CALCULUS

1. Ito calculus: Cartesian coordinates

The following nonlinear stochastic equation with multiplicative noise represents the diffusion process for components of the unit vector $\mathbf{e} = (e_1, e_2, e_3)$ on a sphere:

$$de_i = -2De_i dt + (\delta_{ij} - e_i e_j)\sqrt{2D}dW_j, \tag{A1}$$

$$t = 0, \quad e^2 = \mathbf{e} \cdot \mathbf{e} = 1. \tag{A2}$$

In Eq. (5), the diffusion coefficient $D = T_{\text{Diff}}^{-1}$. Equation (A1) conserves the property Eq. (A2) for any time $t > 0$. Indeed, we have the following sequence of strict transformations for the instantaneous values of e_i:

$$\begin{aligned}
de^2 &= 2e_i de_i + de_i de_i,\\
de^2 &= -4De_i e_i dt + 2e_i(\delta_{ij} - e_i e_j)\sqrt{2D}dW_j + (\delta_{ij} - e_i e_j)(\delta_{ik} - e_i e_k)2DdW_j dW_k,\\
de^2 &= -4Ddt + (\delta_{ij} - e_i e_j)(\delta_{ik} - e_i e_k)2DdW_j dW_k,\\
de^2 &= -4Ddt + (\delta_{kj} - 2e_j e_k + e_j e_j e_k e_k)2D\delta_{jk}dt,\\
de^2 &= -4Ddt + (3 - 2 + 1)2Ddt = 0,
\end{aligned}$$

i.e., if initially $e^2(t = 0) = 1$, then for any instant values of e^2 we have

$$e^2(t > 0) = 1. \tag{A3}$$

2. Stratonovich calculus: Cartesian coordinates

As in Eq. (6), introducing open dot as the Stratonovich product, the stochastic equation for the direction components is this:

$$de_i = (\delta_{ij} - e_i e_j)\sqrt{2D} \circ dW_j. \tag{A4}$$

Equation (A4) conserves the property Eq. (A3) as well. Indeed,

$$\begin{aligned}
de^2 &= 2e_i de_i,\\
de^2 &= 2e_i \circ \sqrt{2D}dW_i - 2e_i e_i e_j \circ \sqrt{2D}dW_j,\\
de^2 &= 2\sqrt{2D}(e_i \circ dW_i - e_j \circ \sqrt{2DdW_j}) = 0.
\end{aligned}$$

Let us remind that the Stratonovich product enjoins the classic rules of the differential analysis and show that Eq. (A4) can be reduced to Eq. (A1). First, note that

$$e_i e_j \circ dW_j = \left(e_i e_j + \tfrac{1}{2}d(e_i e_j)\right)dW_j,$$

and the following expressions are truth:

$$\begin{aligned}
d(e_i e_j)dW_j &= \sqrt{2D}e_j(\delta_{il} - e_i e_l)dW_l dW_j + \sqrt{2D}e_i(\delta_{jk} - e_j e_k)dW_k dW_j,\\
d(e_i e_j)dW_j &= \sqrt{2D}e_j(\delta_{il} - e_i e_l)\delta_{lj}dt + \sqrt{2D}e_i(\delta_{jk} - e_j e_k)\delta_{kj}dt,\\
d(e_i e_j)dW_j &= \sqrt{2D}e_i dt.
\end{aligned}$$

Hence,

$$e_i e_j \circ dW_j = e_i e_j dW_j + \sqrt{2D} e_i dt.$$

Substituting this expression into Eq. (A4), the latter takes the form of Eq. (A1)

3. Presentations by the cross-vector product: Stratonovich calculus, Cartesian coordinates

Equation (A1) can be rewritten in the equivalent form by the cross-vector product:

$$de_i = \sqrt{2D}\epsilon_{ijk} dW_j \circ e_k. \tag{A5}$$

It is worthwhile to note that this stochastic equation is linear; it provides an advantage for the numerical integration. For each component, the expressions from Eq. (A5) are

$$\begin{aligned} de_1 &= \sqrt{D}(dW_2 \circ e_2 - dW_3 \circ e_2), \\ de_2 &= \sqrt{D}(dW_3 \circ e_3 - dW_1 \circ e_3), \\ de_3 &= \sqrt{D}(dW_1 \circ e_1 - dW_2 \circ e_1), \end{aligned} \tag{A6}$$

or in matrix form

$$d\begin{pmatrix} e_1 \\ e_2 \\ e_3 \end{pmatrix} = \begin{pmatrix} 0 & -dW_3 & dW_2 \\ dW_3 & 0 & -dW_1 \\ -dW_2 & dW_1 & 0 \end{pmatrix} \circ \begin{pmatrix} e_1 \\ e_2 \\ e_3 \end{pmatrix}. \tag{A7}$$

It is easy to see from Eq. (A6) that the norm is conserved with the progress of time:

$$\tfrac{1}{2} de^2 = e_i de_i = 0.$$

4. Presentations by the cross-vector product: Ito calculus, Cartesian coordinates

Using Ito's and Stratonovich's definitions, Eq. (A5) can be reduced to its equivalent Ito's form. To show this, note for example that

$$\begin{aligned} dW_2 \circ e_3 &= dW_2 e_3 + \tfrac{1}{2} dW_2 de_3 = dW_2 e_3 - \tfrac{1}{2} e_1 dt, \\ dW_2 \circ e_3 &= dW_3 e_2 + \tfrac{1}{2} dW_3 de_2 = dW_3 e_2 - \tfrac{1}{2} e_1 dt, \end{aligned}$$

and similarly for $dW_3 \circ e_1$, $dW_1 \circ e_3$, $dW_1 \circ e_2$, $dW_2 \circ e_1$. Substituting such expressions into Eq. (A6) yields

$$de_i = -2De_i dt + \sqrt{2D}\epsilon_{ijk} dW_j e_k. \tag{A8}$$

The equivalence between two Ito's formulations, Eqs. (A1) and (A8), can also be demonstrated. To this end, let us rewrite Eq. (A1) for the first component, for example,

$$\begin{aligned} de_1 &= -2De_1 dt + (1 - e_1 e_1)\sqrt{2D} dW_1 - e_1 e_2 \sqrt{2D} dW_2 - e_1 e_3 \sqrt{2D} dW_3, \\ de_1 &= -2De_1 dt + (e_2 e_2 + e_3 e_3)\sqrt{2D} dW_1 - e_1 e_2 \sqrt{2D} dW_2 - e_1 e_3 \sqrt{2D} dW_3, \\ de_1 &= -2De_1 dt + e_2 \sqrt{2D}(e_2 dW_1 - e_1 dW_2) + e_3 \sqrt{2D}(e_3 dW_1 - e_1 dW_3). \end{aligned}$$

The following identity can be proven:

$$(e_2 e_2 dW_1 - e_1 e_2 dW_2) + (e_3 e_3 dW_1 - e_1 e_3 dW_3) = e_3 dW_2' - e_2 dW_3'.$$

Here dW_2' and dW_3' are new standard Wiener processes. Consequently, it is seen that Eq. (A1) for the first component is equivalent to the expression for the first component from Eq. (A8),

$$de_1 = -2De_1 dt + e_3 dW_2' - e_2 dW_3',$$

and so forth for two other components.

5. The relaxation to the presumed direction

Let us consider the Ornstein-Uhlenbeck stochastic process for the unit direction vector $\mathbf{e}$, with relaxation to a presumed direction, denoted here by the unit vector $\mathbf{h}$. In this case, the stochastic equation for $d\mathbf{e}$ admits an additional term: $(\mathbf{h}\times\mathbf{e})\times\mathbf{e}\,dt/T_{\rm rel}$, where $T_{\rm rel}$ is the typical time of relaxation. The cross-vector product $(\mathbf{h}\times\mathbf{e})\times\mathbf{e}$ can be expressed as

$$(\mathbf{h}\times\mathbf{e})\times\mathbf{e} = -(\mathbf{h}-(\mathbf{e}\cdot\mathbf{h})\mathbf{e}) = -\mathbf{h}_\perp,$$

where $\mathbf{h}_\perp$ is the projection of $\mathbf{h}$. Then updated Ito's and Stranovich's forms, Eqs. (A1), (A4), (A5), and (A8), have the following forms:

$$de_i = -(h_i-(h_je_j)e_i)\frac{dt}{T_{\rm rel}} - 2De_idt + (\delta_{ij}-e_ie_j)\sqrt{2D}dW_j, \tag{A9}$$

$$de_i = -(h_i-(h_je_j)e_i)\frac{dt}{T_{\rm rel}} + (\delta_{ij}-e_ie_j)\sqrt{2D}\circ dW_j, \tag{A10}$$

$$de_i = -(h_i-(h_je_j)e_i)\frac{dt}{T_{\rm rel}} + \sqrt{2D}\epsilon_{ijk}dW_j\circ e_k, \tag{A11}$$

$$de_i = -(h_i-(h_je_j)e_i)\frac{dt}{T_{\rm rel}} - 2De_idt + \sqrt{2D}\epsilon_{ijk}dW_je_k. \tag{A12}$$

6. Midpoint scheme: Stratonovich's form [Eq. (A7)]

In time, with set $t_n,\ t_{n+1},\ldots$ the midpoint method, giving a global error of order $O(\Delta t^2)$, advances in two steps. The first one evaluates explicitly the intermediate unit vector $\mathbf{e}^{\rm mid}$:

$$\mathbf{e}^{\rm mid} = \left(\mathbf{I}+\tfrac{1}{2}\mathbf{A}\right)\mathbf{e}^n,$$

where $\mathbf{I}$ is the unit matrix, the matrix $\mathbf{A}$ is given by

$$\mathbf{A} = \sqrt{2D}\begin{pmatrix} 0 & -dW_3 & dW_2 \\ dW_3 & 0 & -dW_1 \\ -dW_2 & dW_1 & 0 \end{pmatrix}.$$

The second (implicit) step provides values $\tilde{\mathbf{e}}^{n+1}$, solving by Kramer's rule the following system:

$$\tilde{\mathbf{e}}^{n+1} = \left(\mathbf{I}-\tfrac{1}{2}\mathbf{A}\right)^{-1}\left(\mathbf{I}+\tfrac{1}{2}\mathbf{A}\right)\mathbf{e}^n.$$

This solution is further updated by the relaxation term—the first term on the right-hand side of Eq. (A11):

$$e_i^{n+1} = \frac{\tilde{e}_i^{n+1}T_{\rm rel}+h_idt}{T_{\rm rel}+\left(h_je_j^n\right)dt}.$$

[1] F. Belin, F. Moisy, P. Tabeling, and H. Willaime, *Worms in a Turbulence Experiment, from Hot Wire Time Series, Trends in Mathematics* (Birkhäuser Verlag, Basel, 1999), pp. 129–140.

[2] G. E. Elsinga and I. Marusic, Universal aspects of smallscale motions in turbulence, J. Fluid Mech. **662**, 514 (2010).

[3] S. Goto, A physical mechanism of the energy cascade in homogeneous isotropic turbulence, J. Fluid Mech. **605**, 355 (2008).

[4] F. Moisy and J. Jimenez, Geometry and clustering of intense structures in isotropic turbulence, J. Fluid Mech. **513**, 111 (2004).

[5] H. Mouri, A. Hori, and Y. Kawashima, Vortex tubes in velocity fields of laboratory isotropic turbulence: Dependence on the Reynolds number, Phys. Rev. E **67**, 016305 (2003).

[6] A. Vincent and M. Meneguzzi, The dynamics of vorticity tubes in homogeneous turbulence, J. Fluid Mech. **258**, 245 (1994).
[7] J. Bec, L. Biferale, G. Boffetta, A. Celani, M. Cencini, A. Lanotte, S. Musacchio, and F. Toschi, Acceleration statistics of heavy particles in turbulence, J. Fluid Mech. **550**, 349 (2006).
[8] S. B. Pope, *Turbulent Flows* (Cambridge University Press, Cambridge, 2000).
[9] J.-P. Minier, On lagrangian stochastic methods for turbulent polydisperse two-phase reactive flows, Prog. Energy Combust. Sci. **50**, 1 (2015).
[10] J.-P. Minier, Statistical descriptions of polydisperse turbulent two-phase flows, Phys. Rep. **665**, 1 (2016).
[11] V. Sabelnikov, A. Chtab-Desportes, and M. Gorokhovski, The coupled LES-subgrid stochastic acceleration model (LES-SSAM) of a high Reynolds number flows, in *Advances in Turbulence XI*, Vol. 117 (Springer, Berlin, 2007).
[12] V. Sabelnikov, A. Chtab-Desportes, and M. Gorokhovski, New sub-grid stochastic acceleration model in LES of high-Reynolds-number flows, Eur. Phys. J. B **80**, 177 (2011).
[13] N. Mordant, A. M. Crawford, and E. Bodenschatz, Three-Dimensional Structure of the Lagrangian Acceleration in Turbulent Flows, Phys. Rev. Lett. **93**, 214501 (2004).
[14] N. Mordant, J. Delour, E. Léveque, A. Arnéodo, and J.-F. Pinton, Long Time Correlations in Lagrangian Dynamics: A Key to Intermittency in Turbulence, Phys. Rev. Lett. **89**, 254502 (2002).
[15] G. A. Voth, A. La Porta, A. M. Grawford, J. Alexander, and E. Bodenschatz, Measurement of particle accelerations in fully developed turbulence, J. Fluid Mech. **469**, 121 (2002).
[16] R. Zamansky, I. Vinkovic, and M. Gorokhovski, Acceleration in turbulent channel flow: Universalities in statistics, subgrid stochastic models, and an application, J. Fluid Mech. **721**, 627 (2013).
[17] M. Gorokhovski and R. Zamansky, Modeling the effects of small turbulent scales on the drag force for particles below and above the Kolmogorov scale, Phys. Rev. Fluids **3**, 034602 (2018).
[18] A. Pumir and M. Wilkinson, Orientation statistics of small particles in turbulence, New J. Phys **13**, 093030 (2011).
[19] M. Wilkinson and A. Pumir, Spherical Ornstein-Uhlenbeck processes, J. Stat. Phys. **145**, 113 (2011).
[20] A. Tsinober, *An Informal Introduction to Turbulence* (Kluwer, The Netherlands, 2001).
[21] F. Toschi and E. Bodenschatz, Lagrangian properties of particles in turbulence, Annu. Rev. Fluid Mech. **41**, 375 (2009).
[22] P. K. Yeung and S. B. Pope, Lagrangian statistics from direct numerical simulations of isotropic turbulence, J. Fluid Mech. **207**, 531 (1989).
[23] P. K. Yeung, S. B. Pope, A. G. Lamorgese, and D. A. Donzis, Acceleration and dissipation statistics of numerically simulated isotropic turbulence, Phys. Fluids **18**, 065103 (2006).
[24] A. S. Monin and A. M. Yaglom, *Statistical Fluid Mechanics: Mechanics of Turbulence* (MIT Press, Cambridge, MA, 1981).
[25] S. B. Pope and Y. L. Chen, The velocity dissipation probability density function model for turbulent flows, Phys. Fluids A **2**, 1437 (1990).
[26] R. S. Rogallo, Numerical experiments in homogeneous turbulence, *NASA Technical Memorandum* (National Aeronautics and Space Administration (NASA), 1981).
[27] R. S. Rogallo and P. Moin, Numerical simulation of turbulent flows, Annu. Rev. Fluid Mech. **16**, 99 (1984).
[28] J. B. Lagaert, G. Balarac, and G.-H. Cottet, Hybrid spectral-particle method for the turbulent transport of a passive scalar, J. Comput. Phys. **260**, 127 (2014).
[29] G. I. Taylor, Diffusion by continuous movements, Proc. London Math. Soc. **2**, 196 (1922).
[30] A. M. Obukhov, Description of turbulence in terms of Lagrangian variables, Adv. Geophys. **6**, 113 (1956).
[31] J. Jung, K. Yeo, and C. Lee, Behavior of heavy particles in isotropic turbulence, Phys. Rev. E **77**, 016307 (2008).
[32] L. Baker, A. Frankel, and F. Coletti, Coherent clusters of inertial particles in homogeneous turbulence, J. Fluid Mech. **833**, 364 (2017).
[33] A. Pumir and M. Wilkinson, Collisional aggregation due to turbulence, Annu. Rev. Condens. Matter Phys. **7**, 141 (2016).